

Proceedings of the ASME 2019 Conference on Smart Materials, Adaptive Structures and Intelligent Systems SMASIS2019 September 9-11, 2019, Louisville, KY, USA

SMASIS2019-5560

ANALYTICAL MODELING AND SIMULATION OF THE BLOCKED FORCE AND LARGE DEFORMATION OF MULTIFUNCTIONAL SEGMENTED LITHIUM ION BATTERY UNIMORPH ACTUATOR

Cody Gonzalez*

Department of Mechanical Engineering The Pennsylvania State University University Park, Pennsylvania 16802 Email: cag46@psu.edu

Mary Frecker

Professor
Department of Mechanical Engineering
The Pennsylvania State University
University Park, Pennsylvania 16802
Email: mxf36@psu.edu

Jun Ma

Department of Mechanical Engineering The Pennsylvania State University University Park, Pennsylvania 16802 Email: jxm1153@psu.edu

Christopher Rahn

Professor
Department of Mechanical Engineering
The Pennsylvania State University
University Park, Pennsylvania 16802
Email: cdrahn@psu.edu

ABSTRACT

A self-powered, and self-actuating lithium ion battery (LIB) has the potential to achieve large deformation while still maintaining The energy storage capability allows for actuation force. continual actuation without an external power source once Reshaping the actuator requires a nonuniform charged. distribution of charge and/or bending stiffness. varying the state of charge and bending stiffness along the length of a segmented unimorph configuration have the effect of improving the tailorability of the deformed actuator. In this paper, an analytical model is developed to predict the actuation properties of the segmented unimorph beam to determine its usefulness as an actuator. The model predicts the free deflection, blocked deflection, and blocked force at the tip as a function of spatially varying state of charge and bending stiffness. The main contribution of the paper is the development of blocked deflection over the length of the segmented unimorph, which has not yet been considered in the literature. The model is verified using experimental data and commercial finite element analysis.

NOMENCLATURE

	-
T_1	uniform stress at material interface
S_1	interfacial strain
E	elastic modulus
${S_I}^*$	induced actuation strain
β	linear strain rate
$\hat{\mathcal{C}}_{Li}$	average normalized concentration of lithium
	ions (state of charge)
EI	equivalent stiffness
v	vertical deflection
M_{eq}	equivalent end moment
x	distance along the length of the beam
L	beam length
F_b	blocked force
κ	curvature
I	area moment of inertia
W	beam width
h_{Ct}	coating layer thickness
h_{Cu}	copper layer thickness
h	neutral axis
U	strain energy
N_{seg}	number of segments

^{*}Address all correspondence to this author

 $M_{eq,N_{seg}_{mod}}$ modified equivalent end moment of the tip segment C constants of integration

1. INTRODUCTION

Lithium-ion batteries (LIB) are ubiquitous and effective devices for energy storage. Besides being capable of energy storage, LIB can be designed as multifunctional devices capable of actuation and sensing when configured in a composite unimorph structure. The unimorph consists of a LIB with a copper current collector coated with an active composite layer of silicon, binder, and conductive agent. The actuation strain is induced by charging the battery, and the actuation stress is proportionally dependent on the state of charge (SOC) such that the maximum deflection of a uniform unimorph occurs at 100% SOC.

In previous work by the authors, an analytical model was developed to predict the free deflection of a segmented LIB unimorph actuator with spatially varying geometry or state of charge [1]. The focus of the current paper is on expansion of the model to include the blocked force and deflection of the segmented LIB unimorph and validation using experimental data and finite element simulation. The experimental data is used to validate the uniform unimorph free deflection and allow for the determination of the optimal linear strain rate while the finite element simulation is used to verify the analytical model of the blocked deflection and blocked force.

The key to achieving large deflection in the LIB unimorph actuator is the lithiation of silicon which causes over 300% volumetric expansion [2]. Embedding Si nanoparticles in the soft composite coating on a layer of copper allows transformation of this volumetric expansion to deflection of the beam. The actuation mechanism is the restrained expansion caused by the copper foil, i.e., while the composite coating layer expands the copper foil is relatively inextensible. This results in the unimorph bending, as seen in Figure 1. As the battery is charged and Li ions are inserted, the Silicon nanoparticles form an alloy with Li creating Li_rSi. This alloying increases the volume of the particle by 310% causing the voids formed during the fabrication of the actuator to shrink and the coating layer to expand longitudinally [2]. The relationship between the volumetric expansion driven by the SOC of the battery is the linear strain rate β .

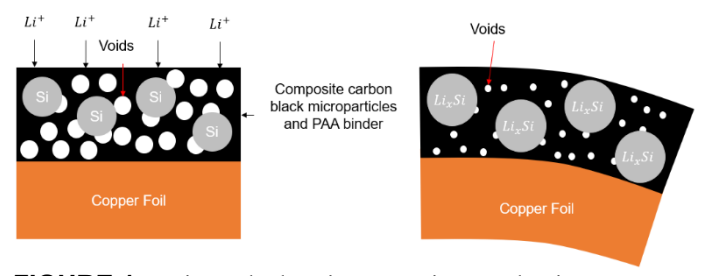


FIGURE 1: Unimorph charging actuation mechanism.

The volume expansion and resulting actuation can be harnessed further by segmenting the unimorph along its length and spatially varying the thickness and SOC. By segmenting the

beam and changing the geometry, SOC, or both, of each segment, complex actuation shapes can be obtained for such tasks as soft robotics gripping. A schematic for spatially varying SOC can be seen in Figure 2, and a schematic for spatially varying geometry can be seen in Figure 3. Figure 2 shows the case where theoretically each segment is electrically insulated and charged separately such that spatially varying SOC (charge varying along the beam length) can be achieved. In the case presented the charge is spatially varied uniformly such that the tip is charged to full 100% SOC while the base segment remains uncharged at 0% SOC. The intermediate segments are charged to fractions of full charge. By varying the SOC of each segment, complex actuation shapes can be achieved. Moreover, the shape of the actuator can be changed by redistributing the charge among the segments costing no additional energy beyond that lost to internal resistance. In this way this LIB actuator may be considered superior to those relying on pneumatic power or those relaying on an externally applied electric of magnetic field.

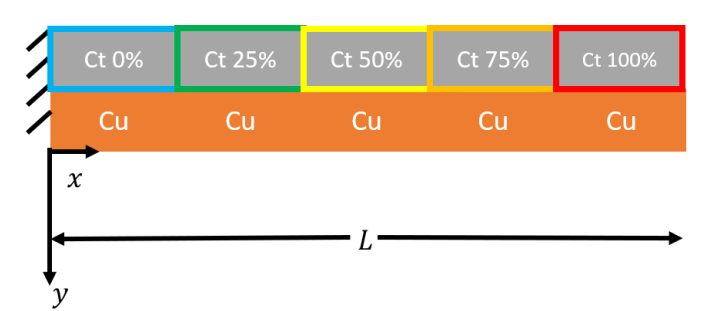


FIGURE 2: Segmented beam with spatially varying SOC.

Further shape complexity can be achieved by spatially varying (along the length of the beam) the geometry of the unimorph. While both the active and passive layer thickness can be varied, here only the passive layer (the copper foil) thickness is varied. Seen in Figure 3, the beam is held at a uniform charge of 100% while the geometry is spatially varied by tapering the thickness of the passive layer toward the tip. In doing so, nonuniform curvature along the length can be achieved. Furthermore, although not studied here, varying both the SOC and the geometry of the beam can provide an optimized design for a specific application.

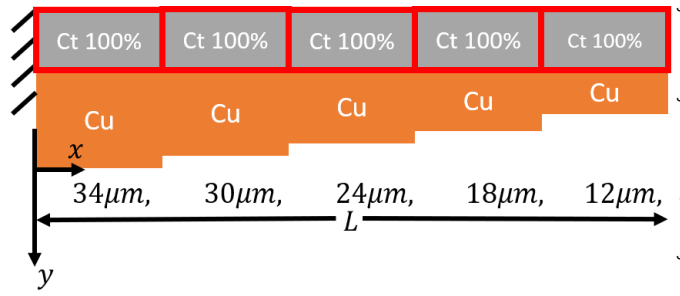


FIGURE 3: Segmented beam with spatially varying SOC.

Because of the nature of the LIB actuation mechanism, large deformation can be achieved while maintaining actuation force. Reshaping, while limited in terms of time scale by lithium diffusion, is also achievable by redistribution of charge. All this can occur while the LIB actuator still acts as a means of energy storage.

The unimorph actuator is modeled as a cantilever composite beam. The performance metrics of interest are the free deflection and blocked force as a function of SOC. While analytical models have been developed to predict free deflection of these types of structures, the deflection during the blocked force condition has not been considered in the literature due to the nonlinear nature of a clamped-roller beam with applied moment and end loading [3–7].

Current methods for solving the large blocked deflection of cantilevered elastica include both shooting methods such as in the work of Holland et al., Banerjee et al., and Phungpaingam et They also include finite element analysis [8], *al.* [8–10]. Adomian decomposition [9], and elliptic integrals [11]. Crawley et al. and Wada et al. discuss the merits of various models for beam actuation as well including Euler-Bernoulli versus a uniform strain model [12,13]. Elliptic integrals and the use of constants to take into account the vertical deflection as a function of the slope of a beam are discussed by Howell [3]. Normally the nonlinearity of the problem can be ignored for beams with small deflections, but this cannot be assumed for elastica. In this paper, an Euler-Bernoulli model for the deflection of a blocked cantilever unimorph is developed and is compared with its commercial FEA simulated equivalent.

2. ANALYTICAL MODEL BLOCKED DEFLECTION AND BLOCKED FORCE

The analytical model of the segmented unimorph actuator is derived based on beam theory accounting for large deflections and the induced axial strain in the coating layer caused by lithium insertion. The free deflection of a clamped-free segmented unimorph has been developed previously [1] and is summarized briefly here. Stress in the unimorph at the interface of the active and passive material layers T_l is:

$$T_1 = E_{ct}(S_1 + S_1^*) \tag{1}$$

where E_{ct} is the elastic modulus of the active coating layer and S_1 is the transverse strain experienced in response to the coating layer axial strain upon lithium insertion, ${S_I}^*$. This actuation strain is assumed to be equal to the product of the normalized average lithium concentration \hat{C}_{Li} and the linear strain rate β (Equation 2). The actuation stress used in the simulation of the deflection of the unimorph is found by multiplying the actuation strain by the elastic modulus of the coating layer.

$$S_1^* = \beta \hat{C}_{Li} \tag{2}$$

2.1 Blocked force for a uniform beam

The blocked force F_b is defined as the reaction force at the tip of the unimorph when the vertical deflection of the tip is constrained to be zero. The blocked force required to prevent tip deflection due to actuation can be calculated for the end of any segment by simulating a cantilever beam with a constrained tip with an equivalent end-moment due to the actuation strain

caused by Li insertion. This statically indeterminate beam can be solved using Castigliano's theorem.

The strain energy due to bending is expressed as U, where M(x) is the internal bending moment and F_b is the blocked force required to prevent deflection at the end of segment i. Castigliano's theorem states the variation of the strain energy with respect to the blocked force is equal to the deflection at the tip, which for a blocked beam is zero, as shown in Equation (3a). Equation (3b) shows the calculated blocked force for a given equivalent end moment where the length of the beam is L.

$$\frac{\partial U}{\partial F_b} = \int_0^L \frac{M}{EI_e} \frac{\partial M}{\partial F_b} dx$$

$$= \frac{1}{EI} \int_0^L \left[(M_{eq} + F_b(x - L))(x - L) \right] dx = 0$$
 (3a)

$$F_b = \frac{3M_{eq}}{2L} \tag{3b}$$

where M_{eq} is the product of the curvature κ and the equivalent bending stiffness of the beam EI (Equation 3d) found using standard analysis of a composite beam found in Equations (3c-3f):

$$M_{eq} = \kappa EI$$
 (3c)

$$EI = E_{Ct}I_{Ct} + E_{Cu}I_{Cu}. (3d)$$

Here the area moment of inertia of the coating layer is:

$$I_{Ct} = \frac{1}{12} w h_{Ct}^3 + w h_{Ct} \left(h_{Cu} + \frac{h_{Ct}}{2} - h \right)^2$$
 (3e)

and the area moment of inertia of the copper foil is:

$$I_{Cu} = \frac{1}{12} w h_{Cu}^3 + w h_{Cu} \left(\frac{h_{Cu}}{2} - h \right)^2$$
 (3f)

2.2 Blocked force for a segmented beam

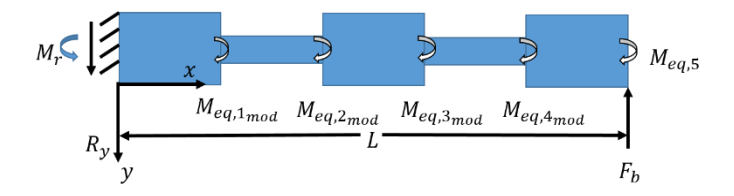


FIGURE 4: Blocked force for a segmented beam using modified equivalent end moments.

For a segmented unimorph, each segment can have its own thickness and SOC and must be considered independently (Figure 4). Here we introduce a modified equivalent end moment for each ith segment, $M_{eq,imod}$ to find the blocked force of the segmented beam.

An expansion of Castigliano's theorem can be seen in Equations (4a-4d) for a beam of N_{seg} segments. The summation of the integral of the product of each segments' internal bending moment and the derivative of the internal bending moment with

respect to blocked force divided by the equivalent stiffness of each respective segment is set equal to zero (Equation 7a) and the blocked force is solved for. The modified equivalent end moment is obtained by subtracting the previous segment's equivalent end moment from the current segment's equivalent end moment. Thus, in Equation (4d), the Nth segment end moment is subtracted from the next segment from the tip (N-1)th. The analytical expression for blocked force follows in Equations (5a-5d).

$$\frac{\partial U}{\partial F_b} = \sum_{i=1}^{N_{seg}} \int_{\frac{(i-1)L}{N_{seg}}}^{\frac{iL/N_{seg}}{N_{i}}} \frac{M_i}{EI_{e_i}} \frac{\partial M_i}{\partial F_b} dx = 0$$
 (4a)

$$M_i = M_{eq_i} + F_b(x - L) \tag{4b}$$

$$M_{eq,N_{seg}_{mod}} = \kappa_{N_{seg}} E I_{N_{seg}} = M_{eq}_{N_{seg}}$$
 (4c)

$$\begin{split} M_{eq,N_{seg}-1_{mod}} &= \kappa_{N_{seg}-1} E I_{N_{seg}-1} - \kappa_{N_{seg}} E I_{N_{seg}} \\ &= M_{eq}_{N_{seg}-1} - M_{eq}_{N_{seg}} \end{split} \tag{4d}$$

Equations (5a-5d) allow for calculation of the blocked force for a beam of N_{seg} segments with spatially varying stiffness and curvature where Equation (5a) is the analytical expression for calculating the blocked force of a segment beam, and the constants are defined in Equations (5b-5d).

$$F_{b} = \frac{\sum_{i=1}^{N_{seg}} \frac{c_{i} \kappa_{i} L^{2}}{a_{N_{seg}}}}{\sum_{i=1}^{N_{seg}} \frac{b_{i} L^{3}}{3N_{seg}^{3} EI_{i}}}$$
(5a)

where:

$$a_{i} = a_{i-1} + 4i - 2$$
: where $m_{1} = 1$;
 $for \ i = 2$: N_{seg} (5b)
 $b_{i} = b_{i+1} - 6i + 6N_{seg}$: where $b_{N_{seg}} = 1$;
 $for \ i = N_{seg} - 1$: 1 (5c)
 $c_{i} = c_{i+1} + 2$: where $c_{N_{seg}} = 1$;
 $for \ i = N_{seg} - 1$: 1 (5d)

2.3 Blocked deflection for a uniform unimorph

In this blocked condition, we are interested in the vertical deflection along the length of the beam, called the blocked deflection. The blocked deflection v(x) for a uniform unimorph can be found at any location along the length of a beam x using Euler-Bernoulli beam theory, where M_{eq} is the equivalent end moment. The vertical deflection can be found using Equation (6):

$$v(x) = \frac{1}{EI} \left(\frac{M_{eq} x^2}{2} + F_b \left(\frac{x^3}{6} - \frac{Lx^2}{2} \right) \right);$$

$$0 \le x \le L$$
(6);

where the blocked force F_b of a uniform beam is found using Equation (3b).

2.4 Blocked deflection for a segmented unimorph

Blocked deflection for a segmented unimorph can be found using standard analysis of a non-prismatic beam coupled with composite beam analysis, accounting for the interfacial conditions between segments.

One can use the deflection of the first segment (Equation 7a) taken and modified from Equation (6) coupled with the slope of the first segment (Equation 7b) to find the constants for the second segment and repeat until the N_{th} segment deflection has been solved for.

$$v_{1}(x) = \frac{1}{EI_{1}} \left(\frac{M_{eq}x^{2}}{2} + F_{b} \left(\frac{x^{3}}{6} - \frac{Lx^{2}}{2} \right) \right)$$

$$0 \le x \le \frac{L}{N_{Seg}}$$

$$v'_{1}(x) = \frac{1}{EI_{1}} \left(M_{eq_{1}}x + F_{b} \left(\frac{x^{2}}{2} - Lx \right) \right)$$

$$0 \le x \le \frac{L}{N_{Seg}}$$
(7b)

The expression for the tip deflection and slope of the first segment can then be set equal to the base of the succeeding segment due to continuity at the interface. A further $2(N_{seg}-1)$ additional equations must be solved to find the constants of the continuity conditions. The continuity equation for deflection at the interface is shown in Equation (8a) and the continuity equation for the slope is shown in Equation (8b).

$$\frac{1}{EI_{i}} \left(M_{eq_{i}} x + F_{b} \left(\frac{x^{2}}{2} - Lx \right) \right) + C_{2,i}$$

$$= \frac{1}{EI_{i+1}} \left(\frac{M_{eq_{i+1}} x^{2}}{2} + F_{b} \left(\frac{x^{3}}{6} - \frac{Lx^{2}}{2} \right) \right) + C_{2,i+1}$$

$$(i - 1) L_{Seg} \le x \le i * L_{Seg}; \qquad (8a)$$

$$\frac{1}{EI_{i}} \left(M_{eq_{i}} x + F_{b} \left(\frac{x^{2}}{2} - Lx \right) \right) + C_{1,i}$$

$$= \frac{1}{EI_{i+1}} \left(M_{eq_{i+1}} x + F_{b} \left(\frac{x^{2}}{2} - Lx \right) \right) + C_{1,i+1}$$

$$(i - 1) L_{Seg} \le x \le i * L_{Seg}; \qquad (8b)$$

where:

$$i = 1: N_{Seg} - 1$$
 (8c)

The constants of integration are solved for using these continuity equations and the deflection can be plotted for the entire unimorph.

2.5 Commercial FEA Simulation

Comsol finite element analysis (FEA) software was used to model the segmented unimorph using overlaid shells. A mesh was then created using these shells with sufficiently many elements to capture the large deformation. Quadratic order elements are used. A Newton solver with constant step iteration was used with linearly elastic materials to solve for the large, geometrically nonlinear deformation. The boundary conditions used in the free deflection of the uniform unimorph were clamped-free and the boundary conditions used in the blocked deflection were clamped-roller with the roller implemented by prescribing zero vertical displacement at the tip while still allowing for nonzero slope and horizontal displacement.

A mesh convergence study was conducted and it was found that for a uniform unimorph of five segments, 30 elements appeared to show mesh convergence in terms of the deflection along the length. Thus, for a five-segment beam, each segment is simulated using 5 elements across the width and 6 elements along the length with a uniform distribution of elements.

With regard to the spatially varying SOC case, the mesh of the uniform unimorph was still deemed suitably dense; however, the spatially varying geometry case required finer meshing around the segment interfaces to capture the large deformation. For the unimorph of spatially varying geometry, a mesh study was conducted and suitable mesh convergence was found for a mesh of 6 elements in width and 10 elements in length per segment with an element ratio of 10 distributed symmetrically in a geometric sequence biased toward the segment interfaces.

3. RESULTS AND DISCUSSION

The free deflection of a uniform unimorph and the blocked deflection and blocked force of a segmented unimorph are simulated using FEA. Previous experimental results [14] are used to validate the analytical model and the FEA simulation of the free deflection of the uniform unimorph. Blocked deflection of a uniform unimorph and a segmented unimorph are simulated to predict the actuation properties of the unimorph actuator under load conditions and used to validate the analytical model. The analytical solution for the blocked force and the resulting blocked deflection of the segmented unimorph with spatially varying geometry or SOC is part of our ongoing work.

The purpose of collecting model and simulation data for the uniform unimorph and comparing it to the experimental data is for validation of the simulation and model. The analytical model was used to predict the free deflection for a unimorph of uniform thickness and state of charge. This unimorph has width (w) of 4mm, unimorph length (l) of 30mm, coating thickness (h_{Ct}) of 6 μ m, copper foil thickness (h_{Cu}) of 34 μ m, coating elastic modulus (E_{Ct}) of 1GPa, and copper elastic modulus (E_{Cu}) of 120GPa. Figure 5 displays data for the analytical model (red), experimental data (green) and experimental data fitted for uniform curvature taken from previous work of the authors [1, 14], along with commercial FEA simulation (black) of the deflection of the uniform unimorph cantilever.

The collection of the experimental data for the uniform unimorph involved the tracking of individual points along the length of the beam using digital image correlation. When assuming uniform curvature in the experimental data, the Y component of the deflection varies no more than 10% from the deflection based on the tracked nonuniform curvature of the beam [14].

The best values of β for the simulation and model were determined based on the minimum root mean square error (RMSE) compared to the raw experimental data. The RMSE is calculated for the vertical deflection predicted by the model and the simulation for various values of β (Table 1). This RMSE is taken over 20 data points of raw experimental data and 100 data points of the data fitted for uniform curvature. While this may skew the error taken due to increased number of data points, a minimum of 100 data points was found to be necessary to achieve accurate prediction of the uniform unimorph.

The highlighted data in Table 1 identify the simulation and model cases that best predict the unfitted experimental data, and these values are displayed in Figure 5. It can be seen that all data clearly overlaps at SOC =20%. However, as the SOC increases an increase in β is needed to match the experimental data. This could be due to plastic deformation that occurs during charging in the experiment. It is also consistent with the fact that the simulation does not require as high a β as does the model because it is better suited at capturing the nonlinear behavior of the deflecting unimorph. As to the efficacy of both simulation and analytical model prediction, neither has larger RMSE than 1 cm compared to the experimental data (fitted and unfitted) for a unimorph length of 30 cm. In fact, at lower states of charge there is less than a single mm of error over the unimorph length.

The commercial FEA simulation for overall deflection along the length agrees best with a lower β at lower SOC. As the SOC is increased, a larger β is needed to accurately predict the unimorph deflection. When the experimental data is fitted for uniform curvature, as has been done in a previous study [14], the requisite β to predict the deflection is higher at $\beta=18\%$ for 40% and 60% SOC. A range of $\beta=18-19\%$ has the best prediction over the range of SOC with a larger β being necessary for larger SOC. While an assumed uniform β is appropriate for this study, as there is no larger RMSE found than 3 cm or 10% over the length, it is possible for other cases that β is not uniform but charge dependent as both the simulation and model data indicate.

TABLE 1: Mean squared error of simulation and model y deflection compared against experimental data.

	Y data (cm)	β=15%	β=16%	β=17%	β=18%	β=19%	β=20%
Simulation vs. raw experimental data	20%SOC	0.0748	0.1867	0.3138	0.4426	0.5727	0.7047
	40%SOC	0.4368	0.2568	0.3358	0.5778	0.8717	1.1836
	60%SOC	0.8744	0.5624	0.7442	1.2900	1.8945	2.5634
Model vs. raw experimental data	20%SOC	0.3029	0.1943	0.0933	0.0721	0.1649	0.2743
	40%SOC	1.0435	0.8086	0.5690	0.3506	0.2500	0.3604
	60%SOC	1.8067	1.4204	1.0327	0.6820	0.5598	0.8663

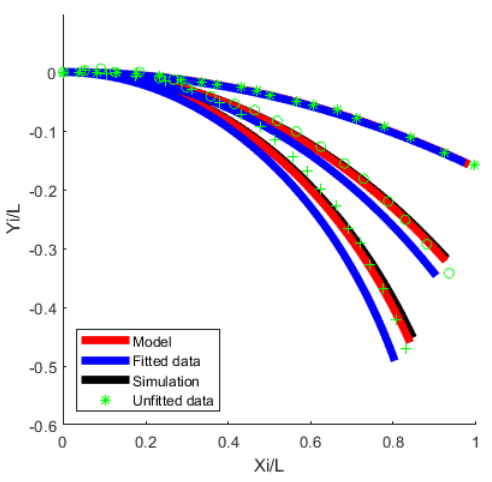


FIGURE 5: Free uniform unimorph model, simulation, fitted experimental data, and unfitted experimental data: SOC = (20.40,60%).

The Euler-Bernoulli analytical model was used to predict the blocked deflection for a unimorph of uniform thickness and state of charge. The unimorph has width (w) 4mm, unimorph length (l) 30mm, coating thickness (h_{Ct}) of 6µm, copper foil thickness (h_{Cu}) of 34µm, coating elastic modulus (E_{Ct}) of 1GPa, and copper elastic modulus (E_{Cu}) of 120GPa. The model assumes a linear strain rate $\beta = 0.20$. Figure 6 displays the blocked deflection using the Euler-Bernoulli model (red) and simulation (black). The simulations are grouped by state of charge with a range of $\beta = 16-19\%$ in increments of 1%. The lowest β has the lowest deflection of a particular grouping, so it can be clearly seen how deflection varies with both β and SOC. The data from the classical beam theory and the simulation appears to agree well as the SOC is increased from 20 to 60% meaning the small deflection assumption is valid for the cases studied.

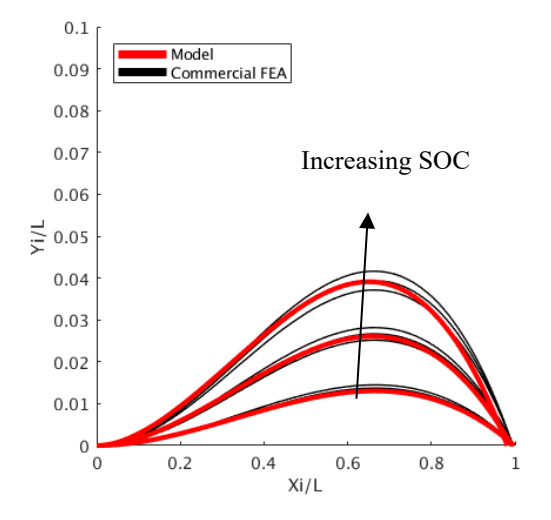
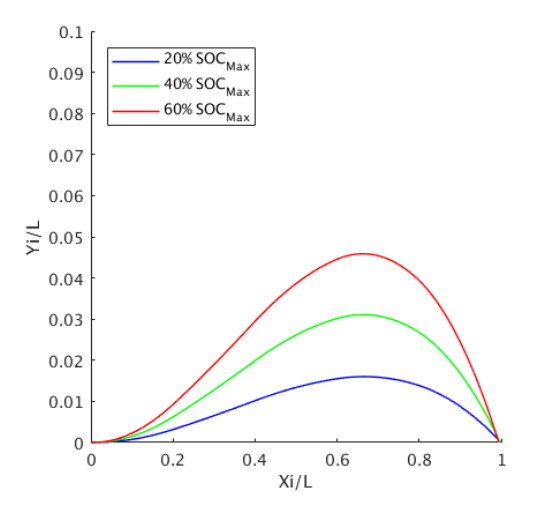


FIGURE 6: Blocked uniform unimorph model, Simulation $\beta = (0.16\text{-}0.18)$; SOC = (20,40,60%).

Figure 7 shows simulation data for deflection along the length of the unimorph for spatially varying SOC. The SOC is varied as follows: A maximum SOC is selected, SOC_{max} , as noted in the Figure. Segment one closest to the root has a 0% SOC, segment two has a 25% of SOC_{max} , segment three has a 50% of SOC_{max} , segment four has 75% of SOC_{max} , and segment five at the tip is fully charged at 100% SOC_{max} . Each segment maintains the same other parameters as the previous examples with segment lengths of 6mm.



unimorph, simulation ($\beta = 0.18$).

Figure 8 displays the FEA simulation of the blocked deflection along the length of the beam for spatially varying thicknesses at constant state of charge. This five-segment unimorph has a length of (l) 30mm, width (w) of 4mm, coating thickness (h_{Ct}) of 6 μ m, coating elastic modulus (E_{Ct}) of 1GPa, and a copper elastic modulus (E_{Cu}) of 120GPa. Segments one through five have respective copper foil thicknesses (h_{Cu}) of: 34, 30, 24, 18, and 12 μ m. Note that the scale of the deflection has been increased to highlight the large deformation of the unimorph despite the blocked tip. This is primarily due to the reduced stiffness caused by tapering the unimorph toward the tip. It can be observed that the deflection near the tip is so large that the simulation predicts that the tip actually rotates past 90 degrees, which may not be possible in practice.

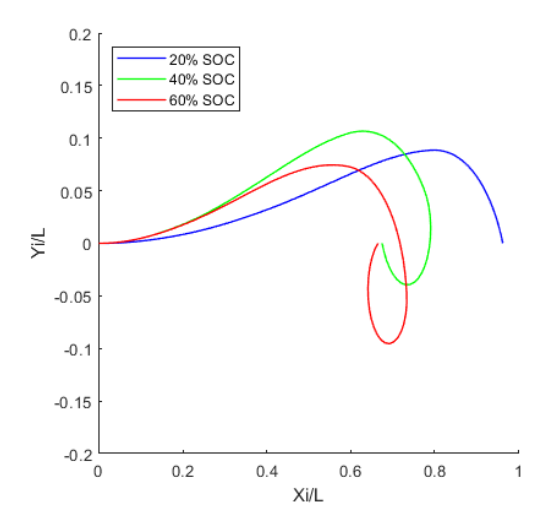


FIGURE 8: Blocked spatially varying geometry unimorph simulation $\beta = 0.18$.

One additional blocked deflection case was considered with the FEA simulation, as shown in Figure 9. This five-segment unimorph has the same properties as the cases discussed in Figure 8 with two exceptions. The unimorph has 60% uniform SOC and the unimorph tapers from a base thickness of 34 μ m to a tip thickness of 30 μ m. The figure is plotted using Comsol plotting software to display the mesh density. It can be observed that the very large rotation of the tip does not occur in this case, which is expected due to the thicker segments and lower SOC.

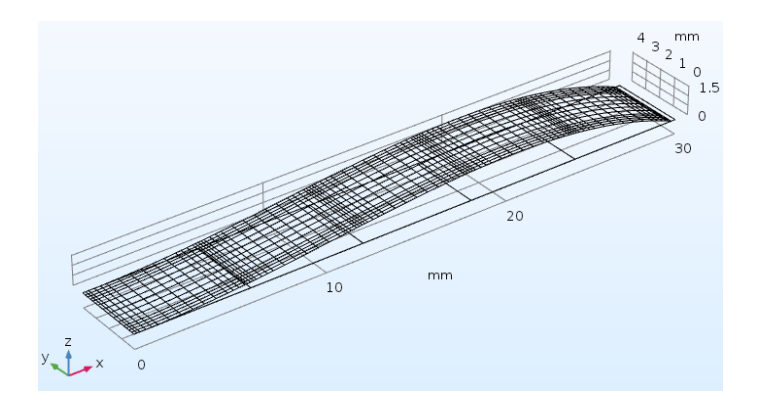


FIGURE 9: Blocked spatially varying geometry unimorph simulation $\beta = 0.18$.

The magnitude of the blocked force, or reaction force when the tip is fixed in the vertical direction, is shown in Figure 10 for the three cases modeled: uniform, spatially varying SOC, and spatially varying geometry. The simulated blocked force assumes β =15% for the uniform case. There is some slight divergence from the model as might be expected since β is assumed to be constant at all SOC. All modeled cases shown assume a β =20%.

It can be seen that the blocked force increases with SOC in all cases, as expected, and that the spatially varying SOC case exhibits the least blocked force. The modeled and simulated uniform case agree well considering that β is assumed to be constant.

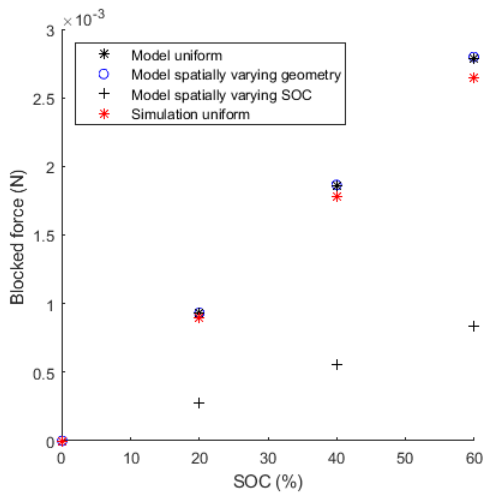


FIGURE 10: Modeled and simulated blocked force at increasing SOC.

4. SUMMARY AND CONCLUSIONS

A lithium ion battery unimorph actuator has the potential to achieve large deflection in complex shapes and is capable of blocked force on the order of mN. Segmenting the unimorph has the potential to achieve even more complex shapes and potentially more blocked force.

Deflection results from experiments, simulations, and an analytical model are compared for a uniform unimorph to provide experimental validation on which to build a model and subsequent simulation for blocked deflection and blocked force.

Spatially varying the SOC and the geometry of the unimorph allows for improved tailorability and generation of complex shapes. A novel derivation for the blocked force of a segmented unimorph has also been derived to potentially supplant its uniform analytical equivalent.

Although the model and simulation are capable of predicting excessive curvature, it is expected that the blocked force in these cases is not accurate. As a result, accurate prediction of blocked force by both the model and simulation is currently restricted to lower SOC and stiffness cases. A combination of high SOC and low stiffness where excessive curvature occurs, results in inaccurate prediction of the blocked force. In a case where no curl over occurs due to sufficiently large stiffness, it may be possible that the increased curvature caused by the drop in stiffness may overcome the decreased blocked force resulting from lowered stiffness. As blocked force is proportional to the sum of the product of the curvature and stiffness as seen in Equation (5a), a tradeoff may be possible and therefore an optimal design may exist at a particular unimorph design.

With complex shapes achieved and the potential for actuation characterized by prediction of blocked deflection and blocked force, applications for human-robot interfaces look more possible as larger forces appear to be achieved by segmenting the unimorph. Potential applications that are interesting for the cases studied include rehabilitation using interfaces between robotic exoskeletons and humans. The ability

of a series of these batteries to reshape by redistributing the charge would be applicable to maintaining uniform pressure between the padding of an exoskeleton and human during locomotion

Future work will compare the blocked deflection of a segmented unimorph predicted with this analytical model with the same predicted by commercial FEA simulation.

ACKNOWLEDGMENTS

The authors gratefully acknowledge the support of the National Science Foundation under Grant No. 1662055.

REFERENCES

- [1] Gonzalez, C., Ma, J., Frecker, M., and Rahn, C., 2018, "Analytical Modeling of a Multifunctional Segmented Lithium Ion Battery Unimorph Actuator," *ASME 2018 Conference on Smart Materials, Adaptive Structures and Intelligent Systems, SMASIS 2018*, p. V002T06A009.
- [2] Beaulieu, L. Y., Eberman, K. W., Turner, R. L., Krause, L. J., and Dahn, J. R., 2001, "Colossal Reversible Volume Changes in Lithium Alloys."
- [3] Howell, L. L., 2001, Compliant Mechanisms, Wiley.
- [4] Low, T. S., and Guo, W., 1995, "Modeling of a Three-Layer Piezoelectric Bimorph Beam with Hysteresis," J. Microelectromechanical Syst., 4(4), pp. 230–237.
- [5] Vel, S. S., and Batra, R. C., 2001, "Analysis of Piezoelectric Bimorphs and Plates with Segmented Actuators," Thin-Walled Struct., **39**(1), pp. 23–44.
- [6] Frecker, M. I., and Aguilera, W. M., 2004, "Analytical Modeling of a Segmented Unimorph Actuator Using Electrostrictive P(VDF-TrFE) Copolymer," Smart Mater. Struct., **13**(1), pp. 82–91.
- [7] Lallart, M., Richard, C., Sukwisut, P., Petit, L., Guyomar, D., and Muensit, N., 2012, "Electrostrictive Bending Actuators: Modeling and Experimental Investigation," Sensors Actuators, A Phys., 179, pp. 169–177.
- [8] Holland, D. B., Stanciulescu, I., Virgin, L. N., and Plaut, R. H., 2006, "Vibration and Large Deflection of Cantilevered Elastica Compressed by Angled Cable," AIAA J., 44(7), pp. 1468–1476.
- [9] Banerjee, A., Bhattacharya, B., and Mallik, A. K., 2008, "Large Deflection of Cantilever Beams with Geometric Non-Linearity: Analytical and Numerical Approaches," Int. J. Non. Linear. Mech., 43(5), pp. 366–376.
- [10] Phungpaingam, B., Athisakul, C., and Chucheepsakul, S., 2009, "Large Deflections of Spatial Variable-Arc-Length Elastica under Terminal Forces," Struct. Eng. Mech., 32(4), pp. 501–516.
- [11] Singh, P., and Goss, V. G. A., 2018, "Critical Points of the Clamped–pinned Elastica," Acta Mech., **229**(12), pp. 4753–4770.
- [12] Crawley, E. F., and Anderson, E. H., 1990, "Detailed Models of Piezoceramic Actuation of Beams," J. Intell. Mater. Syst. Struct., 1(1), pp. 4–25.
- [13] Wada, B. K., Fanson, J. L., and Crawley, E. F., 1990, "Adaptive Structures," J. Intell. Mater. Syst. Struct.,

- **1**(2), pp. 157–174.
- [14] Ma, J., Gonzalez, C., Rahn, C., Frecker, M., and Wang, D., 2018, "Experimental Study of Multifunctional NCM-Si Batteries With Self-Actuation," ASME 2018 Conference on Smart Materials, Adaptive Structures and Intelligent Systems, SMASIS 2018, p. V001T01A009.